# Multiple contact kernel for diffusionlike aggregation

A. Schmitt, G. Odriozola,* A. Moncho-Jordá, J. Callejas-Fernández, R. Martínez-García, and R. Hidalgo-Álvarez†

*Departamento de Física Aplicada, Universidad de Granada, Campus de Fuentenueva, E-18071 Granada, Spain*

(Received 15 October 1999; revised manuscript received 9 June 2000)

The Brownian kernel is usually assumed to describe pure diffusion-limited cluster-aggregation processes. In this work, we show that this assumption is correct for simulated data. For experimental data, however, significant deviations were observed although the system was aggregated at an electrolyte concentration well above the critical coagulation concentration. This indicates that residual cluster-cluster interactions are not completely absent in real experimental systems. In order to improve the description of the experimental data, we developed a kernel that considers a monomer-monomer sticking probability explicitly and accounts for the possibility of multiple monomer-monomer contacts in the cluster collision area. The proposed kernel agrees excellently with the experimental cluster-size distribution and the corresponding scaling function.

PACS number(s): 82.70.Dd, 83.70.Hq, 61.43.Hv, 02.60.Cb

## I. INTRODUCTION

Diffusion-limited cluster aggregation is understood as a regime where the clusters diffuse by pure Brownian motion, and once two clusters collide, they always aggregate [1–3]. This aggregation regime is usually described by the so-called Brownian kernel, which is deduced by solving Fick's equations for freely diffusing spherical particles. The obtained aggregation rates depend on the particle cross section and diffusivity. Fractal concepts are then considered in order to adapt the results obtained for spherical particles to the branched structure of real aggregates. It should be pointed out that the diffusion-limited cluster-aggregation regime models the extremely idealized case in which no interactions between separated particles exist. This means that interparticle interactions are allowed only for the bonds between particles contained within a cluster. In real systems, however, it is very difficult, if not impossible, to eliminate the interactions between distant clusters completely. Consequently, the Brownian kernel is not expected to describe real experimental data precisely and at least small deviations from the ideal diffusion-limited behavior should be observed.

In this paper, we first confirm that the Brownian kernel describes pure diffusion-limited cluster aggregation correctly. For this sake, computer simulations were carried out since this is the only way to ensure that no residual interactions between clusters are present. Second, we fitted the Brownian kernel solution to experimental data obtained for the diffusion-limited cluster aggregation of polystyrene latex particles by means of single cluster light scattering. As expected, significant deviations between experimental and theoretical cluster-size distributions were found. Moreover, the experimental scaling distribution was not well defined in this case. In order to improve the theoretical description of the experimental data, we developed an aggregation kernel that is based on the Brownian kernel and accounts for the effects of residual cluster-cluster interactions by introducing concepts derived from the reaction-limited cluster-aggregation regime.

This paper is structured as follows. Section II is a theoretical background. The formulation of the proposed kernel is presented in Sec. III. In Sec. IV, we describe the materials and methods used for obtaining the experimental and the simulated data. Section V tackles the results and a discussion thereof by comparing the Brownian and the proposed kernel solutions with the experimental and the simulated data. Finally, Sec. VI details the conclusions.

## II. THEORETICAL BACKGROUND

Smoluchowski's equation [4,5]

$$\frac{dN_n}{dt}=\frac{1}{2}\sum_{i+j=n}k_{ij}N_iN_j-N_n\sum_{i=1}^{\infty}k_{in}N_i \tag{1}$$

describes the time evolution of the cluster-size distribution, $N_n(t)$, arising during aggregation of dilute systems. The cluster size, $n$, is defined as the number of individual particles contained within a cluster and $N_n(t)$ as the number of clusters of size $n$. The aggregation kernel, $k_{ij}$, quantifies the rate at which two smaller clusters of size $i$ and $j$ react and form a cluster of size $i+j$. $k_{ij}$ has to be understood as an orientational and configurational average of the exact aggregation rate for two clusters colliding under a specific orientation. All physical information about the aggregation mechanism is contained in the kernel.

### A. Dynamic scaling

Van Dongen and Ernst introduced a classification scheme for homogeneous kernels [6] in terms of two exponents, $\lambda$ and $\mu$, which are defined by the relationship

*Permanent address: Departamento de Química Física y Matemática, Facultad de Química, Universidad de la República, 11800 Montevideo, Uruguay.

†Author to whom correspondence should be addressed. Email address: rhidalgo@ugr.es

 

$$k_{(ai)(aj)} \sim a^{\lambda} k_{ij} \quad (\lambda \leqslant 2)$$
$$k_{ij} \sim i^{\mu} j^{\nu} \quad (\nu \leqslant 1); \quad i \leqslant j; \quad \lambda = \mu + \nu, \tag{2}$$

where $a$ is a positive constant. Kernels with either $\lambda > 2$ or $\nu > 1$ are unphysical, since the cluster reactivity cannot rise faster than its mass. No restrictions are imposed on $\mu$.

The homogeneity parameter $\lambda$ correlates the aggregation rate of two smaller clusters with the aggregation rate of two bigger ones. For $\lambda > 0$, the aggregation rate increases with increasing cluster size and decreases for $\lambda < 0$. Thus, $\lambda$ controls the overall time evolution of the aggregation processes. For $\lambda \leqslant 1$, a cluster of infinite size is formed at infinite time. Only for $1 < \lambda \leqslant 2$ is a gelling behavior observed, i.e., an infinite size cluster is formed at finite time.

The exponent $\mu$ controls the shape of the cluster-size distribution. For negative $\mu$, the big-cluster–small-cluster union is favored and large variations in cluster mass are discouraged. In this case, the cluster-size distribution tends to be tightly bunched, like a bell-shaped curve. For non-negative $\mu$, the union between big clusters is favored and the small clusters are left behind, so that the cluster-size distribution, $N_n$, decreases monotonically for increasing cluster size.

For large clusters and long aggregation times, the solutions of Smoluchowski's equation can be expressed in terms of a time-independent scaling distribution, $\Phi(x)$, as [7,8]

$$N_n(t) \sim s^{-g} \Phi(n/s), \tag{3}$$

where $x = n/s(t)$ can be interpreted as a normalized cluster size. For nongelling systems, mass conservation requires $g = 2$ [8]. The time evolution of the cluster-size distribution is completely contained in the scaling function, $s(t)$, which is related to the number-average cluster-size, $\overline{n_n} = \Sigma_{i=1}^{\infty} i N_i / \Sigma_{i=1}^{\infty} N_i$, by

$$s(t) \sim \overline{n_n} \sim t^{1/(1-\lambda)} \tag{4}$$

for kernels with $\mu < 0$. The functional form of $\Phi(x)$ depends on the exponents $\lambda$ and $\mu$ [8,9].

For the constant kernel, $k_{ij} = k_{11} = \text{const}$, the scaling distribution, $\Phi(x)$, is known in a closed analytical form and given by

$$\Phi(x) = w^2 e^{-wx}, \tag{5}$$

where $w$ is a constant.

### B. Aggregation kernels

It is generally accepted that pure diffusion-limited aggregation of dilute systems may be described by the Brownian kernel. Its analytical form is given by

$$k_{ij} = 4\pi (D_i + D_j)(R_i + R_j). \tag{6}$$

This kernel was derived by considering two solid spheres that approach due to Brownian motion and form a bond as soon as they come into physical contact. The first term on the right-hand side accounts for the diffusive motion of the spheres. Here, $D_i$ and $D_j$ are the diffusion coefficients of sphere $i$ and $j$, respectively. The second term corresponds to the combined collision cross section and is expressed in terms of the sphere radii $R_i$ and $R_j$.

The diffusion coefficient of a sphere is given by the Stokes-Einstein relationship, $D_i = k_B T / 6\pi\eta R$, where $R$ is the radius of the solid sphere, $k_B T$ is the thermal energy, and $\eta$ is the solvent viscosity. Substituting this expression in Eq. (6) yields

$$k_{ij} = \frac{1}{4} k_{11}^{\text{Smol}} (R_i^{-1} + R_j^{-1})(R_i + R_j), \tag{7}$$

where $k_{11}^{\text{Smol}} = 8kT/3\eta$ is the dimer aggregation rate given by Smoluchowski for pure diffusion-limited aggregation [4,5].

In order to adapt the Brownian kernel for two colliding fractal aggregates, an expression for their effective radius and diffusion coefficient had to be found. Computer simulations [10–13] and experiments [14,15] indicated that $D_i = k_B T i^{(-1/d_h)} / 6\pi\eta R_0$ and $R_i = R_0 i^{(1/d_f)}$ are suitable assumptions for colloidal aggregates. Here, $R_0$ is the monomer radius, $d_f$ is the fractal dimension, and $d_h$ is the hydrodynamic fractal dimension. Using these expressions in Eq. (6) yields finally

$$k_{ij} = \tfrac{1}{4} k_{11}^{\text{Smol}} (i^{(-1/d_h)} + j^{(-1/d_h)})(i^{(1/d_f)} + j^{(1/d_f)}). \tag{8}$$

According to Eq. (2), this kernel has

$$\lambda = 1/d_f - 1/d_h \quad \text{and} \quad \mu = -1/d_h. \tag{9}$$

Aggregation kernels for reaction-limited cluster aggregation, proposed in the literature, generally assume the following form:

$$k_{ij} \sim (ij)^{\sigma}, \tag{10}$$

where $\sigma$ is a constant that lies between 0 and 0.5. This type of kernel, however, does not explicitly account for the diffusive motion and the geometrical cross section of the aggregates.

Broide introduced the concept of sticking probability and proposed the following kernel for slow aggregation [16]:

$$k_{ij} \sim (i^{(-1/d_h)} + j^{(-1/d_h)}) P_{ij}. \tag{11}$$

Here, $P_{ij}$ contains the sticking probability for two colliding clusters. He considered $P_{ij}$ to be proportional to the number of monomers contained within a shell of thickness $\Delta R$ near the surface of a cluster. He derived

$$\Delta i \sim \frac{di}{dR} \Delta R \sim i^{(d_f - 1)/d_f} \tag{12}$$

from the relationship $R_i = R_0 i^{(1/d_f)}$, valid for fractal structures. Physically, $\Delta i$ represents the number of ''surface sites'' available for bonding with other clusters. Assuming $P_{ij} \sim \Delta i \Delta j$, he obtained finally

$$k_{ij} \sim (i^{(-1/d_h)} + j^{(-1/d_h)})(ij)^{(d_f - 1)/d_f}. \tag{13}$$

According to Eq. (2), this kernel has $\lambda = 2(d_f - 1)/d_f - 1/d_h$ and $\mu = (d_f - 1)/d_f - 1/d_h$.

The kernel given by Eq. (13) considers explicitly only two effects, cluster diffusion and surface reactivity due to a lim-

ited number of momeric particles contained within the cluster surface. It neglects the geometric cross section of the colliding clusters.

For reaction-limited cluster aggregation, the clusters diffuse and collide just as in the diffusion-limited aggregation regime. However, not every contact results in the formation of a bond. When bonds do form, they are, as in the diffusion-limited aggregation regime, permanent. So, there is no reason for not considering both the diffusive motion and the cross section of the aggregates. In the next section, we propose a kernel that considers these concepts explicitly.

## III. PROPOSING A KERNEL FOR DIFFUSIONLIKE AGGREGATION

The Brownian kernel describes pure diffusion-limited aggregation as a two-step process, i.e., two clusters first approach due to diffusive motion before they react and form a stable bond. Hereby, a physical contact must be established between at least one monomer of each cluster. Since the sticking probability for a single monomer-monomer contact is unity, a stable bond between the clusters is formed independently of the number of monomer-monomer contacts that may exist in the collision area.

For not purely diffusion-controlled aggregation, the clusters diffuse and collide just as in the diffusion-limited regime. However, not every monomer-monomer contact gives rise to the formation of a bond. Now it becomes important to consider the number of monomer-monomer contacts occurring in the collision area. This may be achieved by introducing an additional term, $Q(ij)$, in the Brownian kernel. Taking into account that the sticking probability for a monomer-monomer collision, $p_{11}$, should also be considered, the kernel for not purely diffusion-controlled aggregation becomes

$$k_{ij}=\tfrac{1}{4}k_{11}^{\mathrm{Smol}}p_{11}(i^{(1/d_f)}+j^{(1/d_f)})(i^{(-1/d_h)}+j^{(-1/d_h)})Q(ij). \tag{14}$$

Here, $Q(ij)$ contains the influence of the average number of monomer-monomer contacts contained within the collision region. The product $p_{11}Q(ij)$ is the sticking probability for two colliding clusters. Naturally, when purely diffusion-limited conditions are established, $p_{11}$ and $Q(ij)$ become unity since all contacts between clusters give rise to aggregation and therefore the kernel converts into the Brownian kernel.

In order to obtain an analytical expression for the $Q(ij)$ term, we assume that it should be proportional to the number of monomers per unit area contained within a shell of thickness $\Delta R$ near the surface of each colliding cluster. Considering the fractal structure of the clusters, this number is given by

$$\Delta i/\mathrm{area}\sim\frac{di}{dR}\Delta R/R^2\sim i^{(d_f-3)/d_f}. \tag{15}$$

Hence, $Q(ij)$ may be expressed as

$$Q(ij)=(\Delta i/\mathrm{area})(\Delta j/\mathrm{area})M(ij)=(ij)^{(d_f-3)/d_f}M(ij), \tag{16}$$

where $M(ij)$ is an unknown general function of $i$ and $j$.

$M(ij)$ may be assessed by considering that there is a continuous transition away from the diffusion-limited regime toward the reaction-limited aggregation regime. Consequently, $Q(ij)$ turns unity for purely diffusion-limited conditions, i.e.,

$$1=Q(ij)_{\mathrm{Brown}}=(ij)^{(d_{f_D}-3)/d_{f_D}}M(ij), \tag{17}$$

where $d_{f_D}$ is the fractal dimension for a system aggregating under pure diffusion-limited conditions. Solving for $M(ij)$ and substituting the result into Eq. (16) yields finally

$$Q(ij)=(ij)^{3(d_f-d_{f_D})/d_fd_{f_D}}. \tag{18}$$

Hence, Eq. (14) becomes

$$k_{ij}=\frac{k_{11}}{4}(i^{(1/d_f)}+j^{(1/d_f)})(i^{(-1/d_h)}+j^{(-1/d_h)})(ij)^{3(d_f-d_{f_D})/d_fd_{f_D}}, \tag{19}$$

where $k_{11}$ is $k_{11}^{\mathrm{Smol}}p_{11}$. According to Eq. (2), this kernel has

$$\lambda=6(d_f-d_{f_D})/(d_fd_{f_D})+1/d_f-1/d_h,$$

$$\mu=3(d_f-d_{f_D})/(d_fd_{f_D})-1/d_h. \tag{20}$$

## IV. MATERIALS AND METHODS

Two different techniques were employed for obtaining diffusion-limited aggregation data. On the one hand, computer simulations were carried out. On the other hand, aggregation of polystyrene microspheres was monitored by means of single-cluster light scattering. Afterwards, the obtained data were fitted by the numerical solutions of Smoluchowski's rate equation for the Brownian, the constant, and the proposed kernel. The following subsection describes the simulation process. The next subsection details the main characteristics of the experimental system as well as the operational principle of the single-cluster light-scattering technique. Finally, the numerical procedure to solve Smoluchowski's rate equations and the fitting criteria are summarized.

### A. Simulation

The simulations were carried out by placing randomly $N_0$ identical particles inside a three-dimensional square box. The only imposed restriction was to avoid particle overlapping. The movement of the different aggregates was carried out in the following way.

(i) The monomeric particles are always moved a fixed distance $l_0$ in a random direction.

(ii) The $i$ size clusters ($i>1$) are moved the same distance $l_0$ in a random direction when a generated random number $\xi$ uniformly distributed in [0,1] is less than the ratio between the diffusion coefficients of the $i$ size cluster, $D_i$, and the monomer, $D_m$, i.e. for $\xi<D_i/D_m$.

(iii) The ratio $D_i/D_m$ is calculated assuming that $D_i\sim i^{-1/d_f}$ and so, $D_i/D_m=i^{-1/d_f}$.

(iv) The time step is calculated as $t=l_0^2/6D_m$ where $D_m=k_BT/6\pi\eta R_m$ is the Stokes Einstein translational diffusion

coefficient for a monomer. Here, $\eta$ is the solvent viscosity, $k_BT$ is the thermal energy and $R_m$ is the monomer radius [17].

A collision is considered to occur when a moved cluster overlaps with another one. Since diffusion-limited cluster aggregation is simulated, every collision leads to the formation of a stable bond. The position of the moved cluster is corrected backwards in the direction of the movement so that only the cluster surfaces remain connected. The new cluster continues the movement in the next step. The simulations are off-lattice. Periodic boundary conditions are considered.

### B. Experiment

The experimental cluster-size distributions were obtained from aqueous suspensions of polystyrene microspheres that were aggregated at high electrolyte concentration. The polystyrene particles were manufactured at the laboratories of Granada University. Transmission electron microscopy (TEM) was used to check the particle size and shape. The obtained average particle diameter and polydispersity index were $(638\pm4)$ nm and 1.004, respectively. Sulfate groups derived from the initiator molecules for the polymerization reaction stabilize the particles by charge. The particle surface charge density was determined by conductimetric titration obtaining $(-54\pm2)$ mC/m$^2$. The critical coagulation concentration of $(180\pm7)$ mM was measured by small-angle nephelometry.

The single-cluster light-scattering instrument used for this study is basically a counter and classifier of clusters. It allows the cluster-size distribution up to heptamers and the total concentration of clusters to be measured during a reduced time interval. So, the time evolution of the cluster-size distribution and the number-average cluster size, $\overline{n_n}$, can be obtained by measuring at different stages of the aggregation process. Its principle of operation is based on hydrodynamic focusing of the aggregating sample so that the clusters are forced to flow one by one across a focused laser beam. As they pass, they scatter a pulse of light that is detected at small scattering angle. Under these conditions, the light pulse intensity is directly related to the cluster size and therefore the cluster-size distribution can be obtained by simply counting the pulses as a function of their intensity. Further details of the experimental technique can be found elsewhere [18,19].

Prior to the experiments, the samples were diluted to twice the desired particle concentration and sonicated for 10 min in order to approach monomeric initial conditions. Immediately afterwards, the coagulation process was started by mixing equal volumes of sample and electrolyte solution with a Y-shaped mixing cell. The initial particle concentration was set to $8.0\times10^{13}$ m$^{-3}$ in order to guarantee the proper detection of individual aggregates. The electrolyte concentration was 1.0 M potassium bromide (KBr). The temperature was stabilized at $(21\pm1)$ °C. Pure water was obtained by reverse osmosis followed by percolation through charcoal and a mixed bed of ion-exchange resins. The initial cluster-size distribution was measured for a stable, electrolyte-free sample. The fraction of particles associated in doublets was less than 0.3% in the initial suspension. Larger aggregates were not detected.

### C. Solving Smoluchowski's rate equation

The method described in Ref. [20] was used for solving Smoluchowski's rate equation. It is based on a second-order Runge-Kutta algorithm that solves a limited number of coupled first-order differential equations for a given kernel and initial size distribution. The influence of larger clusters is neglected during the first iteration run. For the following steps, their influence is considered by introducing dynamic scaling concepts. This method presents not only a high degree of precision but is also a fast way to obtain the time evolution of the cluster-size distribution numerically. The experimental data were fitted by minimizing a $\delta$ function defined as

$$\delta=\sqrt{\frac{1}{2IJ}\left[\sum_{j=1}^{J}\sum_{i=1}^{I}\xi_{ji}^2+J\sum_{i=1}^{I}\xi_{\overline{n_n}i}^2\right]}, \tag{21}$$

where $\xi_{ji}$ is the relative deviation between the experimental point $i$ of curve $j$ and the corresponding numerical solution. $\xi_{\overline{n_n}i}$ is defined accordingly for the time evolution of the number-average cluster size, $\overline{n_n}$. $I$ is the total number of experimental points and $J$ is the total number of curves. $\delta$ expresses the square root of the mean quadratic relative deviation. Please note that the number-average cluster-size curve is included in the $\delta$ function and weighted $J$ times in order to consider also the contribution of larger aggregates.

In order to simplify the fitting procedure, the following assumptions were adopted.

(i) Since computer simulations as well as experimental evidence indicate that the fractal dimension, $d_f$, and the hydrodynamic fractal dimension, $d_h$, are approximately equal, $d_f$ and $d_h$ were considered to be identical [21,22].

(ii) The fractal dimension, $d_{f_D}$, for pure diffusion-limited aggregation is assumed to be $(1.75\pm0.05)$. As will be discussed later, this value is widely accepted in the literature but is in no way a general result [11,13,23,24].

This leaves only $k_{11}$ and $d_f$ as fitting parameters for both the Brownian and the proposed kernel [see Eqs. (8) and (19)]. For the computer-generated cluster-size distribution, however, interparticle interactions are completely absent and therefore $k_{11}$ must be $k_{11}^{\mathrm{Smol}}$. Consequently, only $d_f$ is left as a free fitting parameter for the simulated data.

## V. RESULTS AND DISCUSSION

In this section, the numerical algorithm for solving Smoluchowski's rate equation will be used to fit the obtained simulated and experimental data. It will be shown that the Brownian kernel is in excellent agreement with the simulated diffusion-limited aggregation data but it is not capable of fitting the experimental data satisfactorily. Afterwards, the proposed kernel is fitted to the experimental data and a full comparison with the numerical solutions for different aggregation kernels is made.

### A. Simulation

In order to obtain reliable statistics, the simulations were carried out with an initial number $N_0=30\,000$ monomeric particles. The ratio between the total particle volume and the

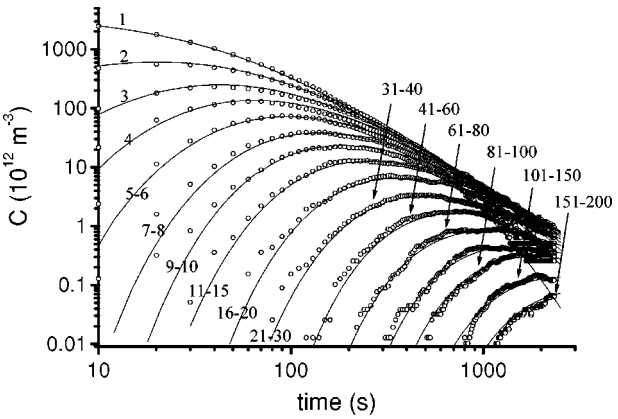


FIG. 1. Time evolution of the cluster concentrations represented in a double-logarithmic scale. The points correspond to the computer-simulated data for monomers up to 200-mers grouped in logarithmically spaced intervals as indicated in the plot. The solid lines represent the fitted numerical solution for the Brownian kernel.

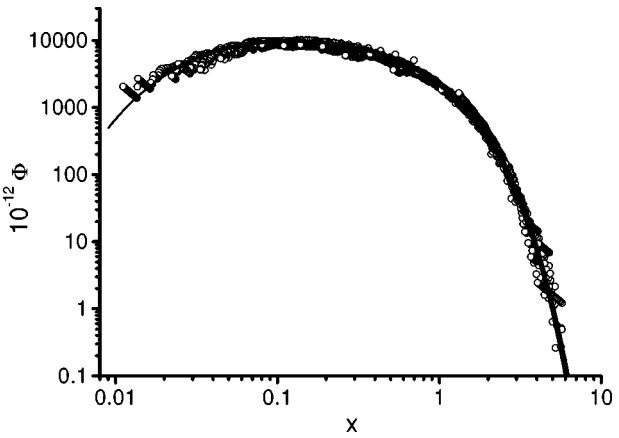


FIG. 2. Simulated dynamic scaling distribution, $\Phi(x)$, for monomers up to 200-mers. The points correspond to the simulated data. The solid line shows the numerically obtained scaling distribution for the Brownian kernel.

box volume was $5\times10^{-4}$. A simulation step length of $l_0=0.4$ times the particle radius was established. In order to calculate the simulation time step, the monomer diameter was chosen as 630 nm, just as for the experiments. For the same sake, the solvent viscosity and the thermal energy were evaluated at 21 °C. The cluster-size distribution, obtained under these conditions, is plotted in Fig. 1 in a double-logarithmic scale. As can be observed, the monomer number decreases monotonously since the individual particles disappear as they react and form bigger aggregates. The curves for all larger aggregates exhibit a maximum as they must first be formed before they can react. For long aggregation times, the curves for smaller aggregates cross the curves for the bigger ones. This behavior is typical for diffusion-limited aggregation. The solid lines in Fig. 1 correspond to the fitted numerical solution for the Brownian kernel. The fitting procedure was performed by considering 16 curves ($J=16$) and a total number of 235 data points per curve ($I=235$). The best fit was obtained for $d_f=(1.73\pm0.09)$. The fitting error was estimated assuming a 5% confidence interval for the $\delta$ function. As can be seen, the agreement between the simulated data and the given solutions for the Brownian kernel is excellent.

In order to corroborate the fitted value for the cluster fractal dimension, we calculated this parameter also from the structure of the simulated clusters by the radius of gyration method described in Ref. [25]. The obtained value, $d_f=(1.72\pm0.03)$, is in good agreement with the fractal dimension calculated from the kinetic data and with those reported in the literature.

Figure 2 shows the dynamic scaling distribution, $\Phi(x)$, calculated for monomers up to 200-mers. The data points correspond to the simulated data. The solid lines represent the numerical solution obtained for the Brownian kernel. It can clearly be seen that the simulated data points define a single master curve that is well described by the numerical solution. It should be pointed out that even the smaller clusters exhibit dynamic scaling behavior at relatively short times. This is quite surprising since the scaling theory is strictly valid only for large clusters at long times. A similar behavior was already reported in the literature [18,26]. As expected, both the numerical and the simulated dynamic scaling distributions show a bell-shaped form that peaks at approximately $x=0.1$. This is in good agreement with the results obtained by Broide and Cohen [9] and Thorn and Seesselberg [27].

### B. Experimental data

In order to obtain experimental data for diffusion-limited colloidal aggregation, a freshly prepared particle suspension was aggregated at 1.0 M potassium bromide (KBr). The electrolyte concentration was chosen well above the critical coagulation concentration so that the sample can safely be assumed to aggregate in the fastest possible aggregation regime.

Figure 3 shows the time evolution of the cluster-size distribution for monomers up to heptamers in a double-logarithmic scale. As for the simulations, the monomer concentration decreases monotonously while the curves for all larger aggregates exhibit a maximum. For longer times, the monomer curve also seems to cross the curves of the bigger aggregates. The experimentally obtained time evolution of the number-average cluster size, $\overline{n_n}$, is plotted in Fig. 4 in a double-logarithmic scale.

#### *1. Fitting the Brownian kernel*

We first fitted the Brownian kernel solution for a cluster fractal dimension of $d_f=1.75$. Figure 5 shows the square root of the mean quadratic relative deviation, $\delta$, defined by Eq. (21), as a function of the fitting parameter $k_{11}$. The calculations were performed for aggregates up to heptamers ($J=7$) and a total number of 67 data points per curve ($I=67$). As can be seen, a well-defined minimum is reached for $k_{11}^{\mathrm{Brown}}=(7.0\pm0.3)\ 10^{-18}\ \mathrm{m^3\,s^{-1}}$. The corresponding numerically calculated cluster-size distribution is plotted together with the experimental data in Fig. 3(a). A relatively good agreement between the fitted curves and the experimental data is observed. The experimental data for the monomeric particles, however, differ quite significantly from the fitted solution. Furthermore, a slight positive deviation

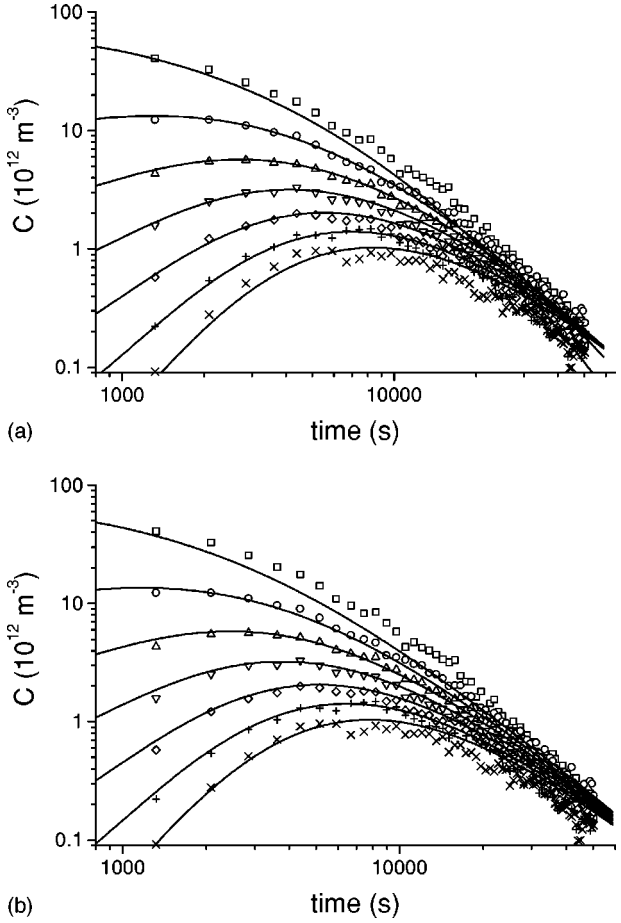


FIG. 3. Time evolution of the concentration of (□) monomers, (○) dimers, (△) trimers, (▽) tetramers, (◇) pentamers, (+) hexamers, and (×) heptamers represented in a double-logarithmic scale. The solid lines in (a) and (b) represent the fitted numerical solutions for the Brownian kernel having $d_f = 1.75$ and the constant kernel, respectively.

can also be perceived for the larger cluster sizes. The dashed line in Fig. 4 shows the numerically calculated time evolution of the number-average cluster size. Here, it can be observed that the numerical solution is unable to fit either the short- or the long-time behavior of the experimental data correctly.

In order to improve the fit, we varied also the cluster fractal dimension $d_f$. We found, however, that the differences between the fitted and the experimental curves diminish slightly for increasing $d_f$ so that the best fit would have been obtained only for the limiting case of $d_f \rightarrow \infty$. Although fractal dimensions higher than the dimension of space are nonphysical, it is interesting to discuss this pathological case in more detail since the Brownian kernel converts into the constant kernel as $d_f$ tends to infinity. For this purpose, Fig. 5 shows also the square root of the mean quadratic relative deviation $\delta$ for the constant kernel. As can be seen, the $\delta$ function reaches a deeper minimum than in the case of the Brownian kernel with $d_f = 1.75$. Now, the best fit for the dimer formation rate constant becomes $k_{11}^{\mathrm{const}} = (8.0 \pm 0.3) \times 10^{-18}$ $\mathrm{m^3\,s^{-1}}$. Nevertheless, the corresponding numerical solutions are not very different from the previous fit (see Figs. 3 and 4). This makes it clear that the Brownian kernel solutions are almost unaffected by variations in the cluster

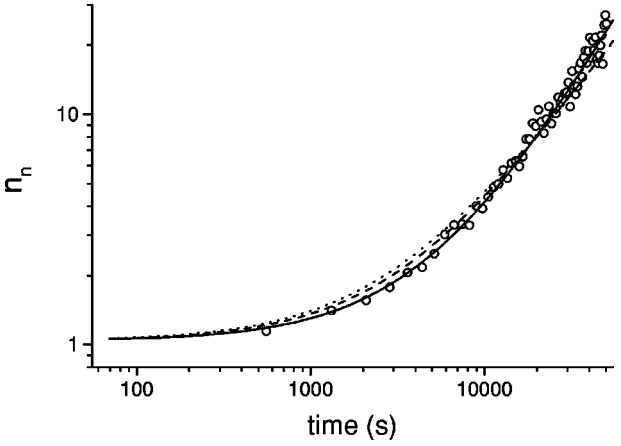


FIG. 4. Time evolution of the number-average cluster size, $\overline{n_n}$. The solid line represents the fitted numerical solution for the proposed kernel. The dashed and the dotted lines correspond to the fitted numerical solutions for the Brownian and the constant kernel, respectively.

fractal dimension, $d_f$. The main difference between both solutions is that the crossing of the different cluster-size curves is only observed for the Brownian kernel solutions. The discrepancies between the obtained $k_{11}$ values can be understood in terms of the kernel shape (see Ref. [20]). Notwithstanding, both values agree with the average dimer formation rate, $\langle k_{11} \rangle = (6 \pm 3) \times 10^{-18}$ $\mathrm{m^3\,s^{-1}}$, determined by Sonntag and Strenge for diffusion-limited cluster aggregation [3]. Their value was calculated by compiling a large set of experimental measurements. It should be pointed out that the experimental values obtained for $k_{11}$ under diffusion-limited conditions are substantially smaller than the theoretical von Smoluchowski value $k_{11}^{\mathrm{Smol}} = 11.1 \times 10^{-18}$ $\mathrm{m^3\,s^{-1}}$ for 21 °C. This discrepancy is generally explained in terms of hydrodynamic interactions, which typically reduce the aggregation rate by a factor of 2 [28–30].

Figure 6 shows the dynamic scaling distribution, $\Phi(x)$, calculated for monomers up to heptamers. The points show the experimental data. The solid line corresponds to the numerical solution obtained for the Brownian kernel having

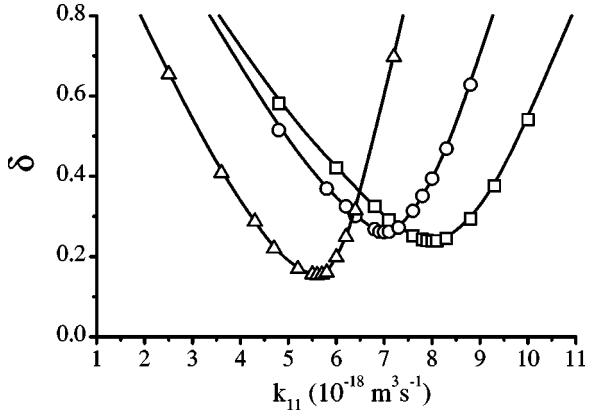


FIG. 5. Square root of the mean quadratic relative deviation, $\delta$, as a function of the fitting parameter, $k_{11}$. The symbols (○), (□), and (△) represent the data for the Brownian kernel having $d_f = 1.75$, the constant, and the proposed kernel, respectively. The continuous lines are drawn as a guide to the eye.

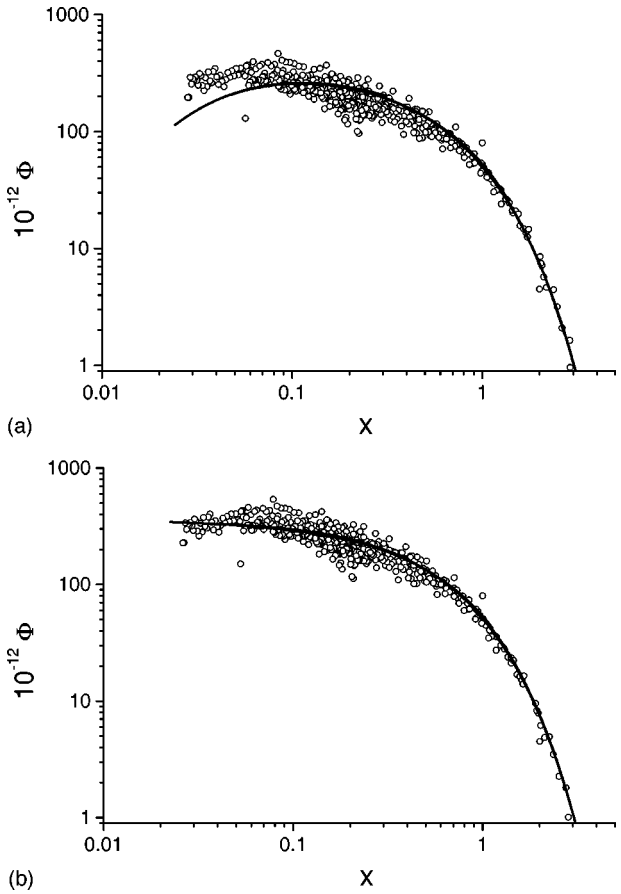


FIG. 6. Dynamic scaling distribution, $\Phi(x)$, calculated for monomers up to heptamers. The points correspond to the experimental data. The solid lines correspond to the numerically obtained scaling distribution calculated for the Brownian kernel having $d_f = 1.75$ (a) and the constant kernel (b).

$d_f = 1.75$ [Fig. 6(a)] and the constant kernel [Fig. 6(b)]. For large arguments, $x$, the experimental data points define a single master curve, which is well described by the numerically obtained dynamic scaling distribution. For small arguments, $x$, the experimental data scatter in a cloud. Also in this region, the numerically calculated scaling distributions fit the experimental data quite well. As expected, the monotonously decreasing shape of the numerically obtained scaling function, $\Phi(x)$, for the constant kernel is perfectly described by the theoretical expression (5). This is why the corresponding curve is not included in Fig. 6(b). The numerically obtained dynamic scaling distribution for the Brownian kernel, however, shows the typical bell-shaped form.

#### *2. Fitting the proposed kernel*

As in the case of the constant and the Brownian kernel, the square root of the mean quadratic relative deviation, $\delta$, was minimized for fitting the proposed kernel given by Eq. (19). The best fit was obtained for $k_{11}^{\mathrm{prop}} = (5.6 \pm 0.2) \times 10^{-18}\ \mathrm{m^3\,s^{-1}}$ and $d_f = (1.87 \pm 0.03)$. Figure 5 shows the corresponding $\delta$ values as a function of the fitting parameter $k_{11}$. The fitted $k_{11}$ value is also in good agreement with the average value determined by Sonntag and Strenge. The $\delta$-function minimum is, however, substantially deeper than the corresponding minima for the constant and the Brownian kernel. This means that the proposed kernel fits the experimental data significantly better. This can clearly be seen in Figs. 4 and 7, which show that the calculated time evolution of the cluster-size distribution and the number-average cluster size for this kernel are in excellent agreement with the experimental data. In this case, no significant deviations are observed.

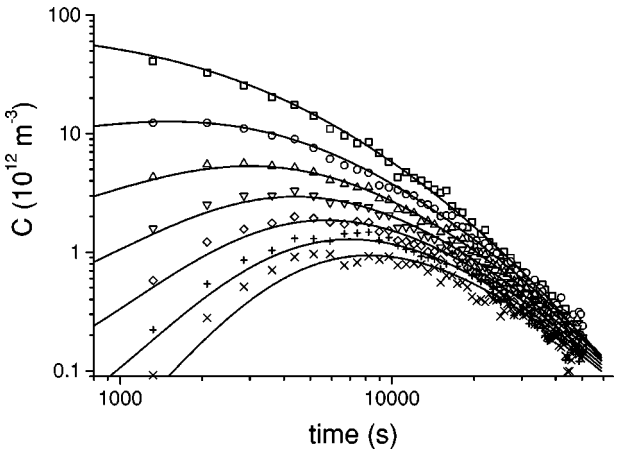


FIG. 7. Time evolution of the concentration of (□) monomers, (○) dimers, (△) trimers, (▽) tetramers, (◇) pentamers, (+) hexamers, and (×) heptamers represented in a double-logarithmic scale. The solid lines represent the fitted numeric solutions for the proposed kernel.

It should be pointed out that the physical interpretation of the fitted value for the fractal dimension, $d_f = (1.87 \pm 0.03)$, is not straightforward. First of all, the given error is determined only as a fitting confidence interval. The proposed kernel depends, however, critically on the difference $(d_f - d_{f_D})$ and so the experimental error of $d_{f_D}$ must also be considered. Taking into account that the $d_{f_D}$ values found in the literature vary usually from 1.7 to 1.8, a better estimation of $d_f$ would be $d_f = (1.87 \pm 0.09)$. On the other hand, it is necessary to keep in mind that the fitted $d_f$ value was obtained from kinetic data and not directly from structural measurements, and therefore implicit assumptions such as the absence of internal cluster rearrangement or multifractality were made. When these effects are present, fractal dimensions even as high as 2.4 are reported for diffusion-limited aggregation processes [26]. This makes it clear that the presented fitting procedure should not be considered as a new independent way to determine the fractal dimension.

The dynamic scaling distribution, $\Phi(x)$, for the proposed kernel is shown in Fig. 8. As for the constant and Brownian kernels, monomers up to heptamers were taken into account. An excellent experimental scaling behavior for the complete measuring interval is observed. The experimental data points line up on the fitted curve almost perfectly. This means that the experimental data scale much better for the proposed kernel. As in the case of the Brownian kernel, the numerically obtained dynamic scaling distribution is bell-shaped. It peaks, however, at approximately $x = 0.03$. The agreement between the numerical and the experimental scaling distribution is excellent. As in the other cases, the numerical solutions scale already during early stages of aggregation.

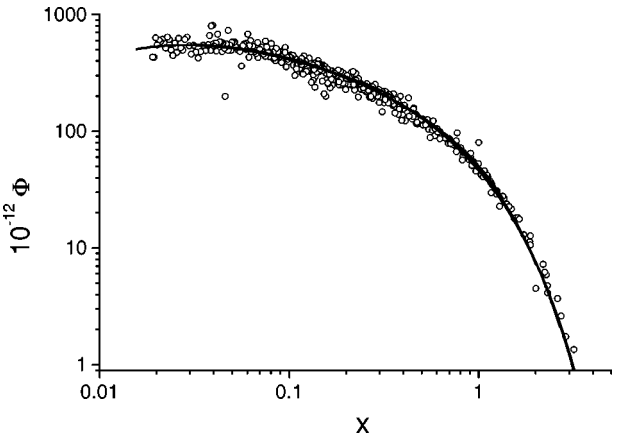


FIG. 8. Dynamic scaling distribution, $\Phi(x)$, obtained for monomers up to heptamers. The points correspond to the experimental data. The solid line corresponds to the numerically obtained scaling distribution for the proposed kernel.

### C. Discussion

The Brownian kernel was employed for fitting aggregation data simulated in the absence of any interactions between distant clusters. Since an excellent agreement between the simulated data and the numerical solutions was obtained, the Brownian kernel can safely be assumed to be an excellent model for pure diffusion-limited cluster aggregation. This suggested, however, that the Brownian kernel may not be capable of describing real diffusion-limited aggregation data where the effects of residual interactions between clusters may have to be considered. We confirmed this assumption by comparing the Brownian kernel solution with experimental data obtained for aqueous suspensions of polystyrene particles aggregating at high electrolyte concentration. Significant deviations were observed not only for the time evolution of the cluster-size distribution but also for the number-average cluster size.

So, an alternative kernel had to be proposed that explicitly accounts for the sticking probability and the possibility of multiple monomer-monomer contacts in the cluster collision area. The improvement with respect to the Brownian and constant kernel solutions were clearly shown not only by the excellent agreement between the experimental and numerically calculated cluster-size distribution, but also by the better defined experimental scaling function, $\Phi(x)$. Furthermore, the deeper minimum obtained for the $\delta$ function confirmed the improvement.

For the fitted monomer reaction rate constants, we obtained $k_{11}^{\mathrm{prop}}<k_{11}^{\mathrm{Brown}}<k_{11}^{\mathrm{const}}$. This finding may be understood by comparing the shape of the corresponding kernel. Figure 9 shows the Brownian kernel as a function of the cluster size in a three-dimensional plot. As can be seen, the main diagonal has slope zero, which means that the corresponding matrix elements, $k_{i=j}$, are constant. Moreover, all matrix elements not too far from the main diagonal are also almost constant. Only the matrix elements close to the axes have significantly higher values. Figure 10 shows the proposed kernel in a similar plot. Although the shape of this kernel is not very different from the shape of the Brownian kernel, it exhibits a main diagonal with a positive slope that is larger for small cluster sizes. Consequently, the ratio $k_{11}/k_{22}$ for the

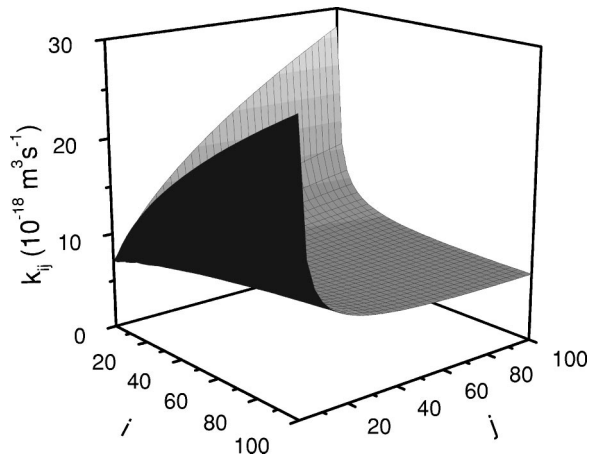


FIG. 9. The Brownian kernel as a function of the cluster size $i$ and $j$.

proposed kernel is smaller than for the Brownian kernel. For this reason, the solution for the proposed kernel yields a slower monomer reaction rate keeping similar values for bigger aggregates. Similar arguments are valid for the comparison of the constant kernel with the Brownian kernel [20].

In the result section, it was also shown that the experimentally obtained dynamic scaling distribution is best defined for the proposed kernel. This is a consequence of the different $\lambda$ values for the corresponding kernels. For the Brownian kernel, Eq. (9) yields $\lambda=0$ and $\mu=-0.57$. Considering the fitted $d_f$ value, $\lambda=0.22$ and $\mu=-0.42$ were obtained from Eq. (20) for the proposed kernel. The constant kernel has $\lambda=0$ and $\mu=0$. $\lambda$ determines the shape of the scaling function, $s(t)$, which, according to Eq. (3), is needed for calculating the dynamic scaling distribution, $\Phi(x)$. Hence, $\lambda$ controls the scaling behavior of the cluster-size distribution. The fact that $\Phi(x)$ is best defined for $\lambda=0.22$ makes it clear that the system is almost but not purely diffusion-controlled.

It should be pointed out that also Thorn and Seesselberg detected discrepancies between the Brownian kernel solution and experimental data for diffusion-limited cluster aggregation [9,27]. They conclude that ‘‘ . . . the purely Browninan kernel has to be modified in such a way that large clusters

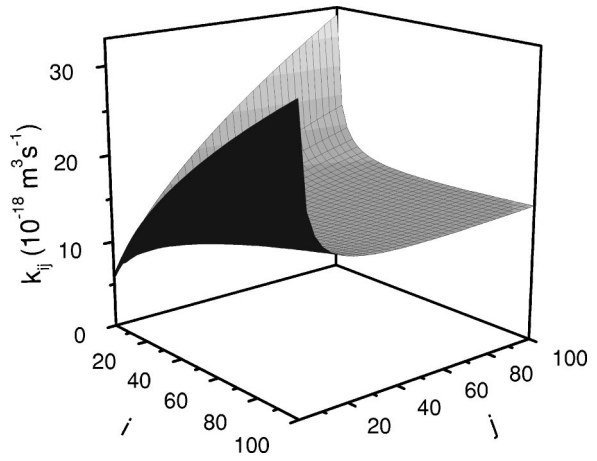


FIG. 10. The proposed kernel as a function of the cluster size $i$ and $j$.

have a higher collision rate . . . '' for improving the kinetic description of the experimental data. As a possible reason for this effect, they suggest differential settling. The aggregation kernel proposed in this paper also predicts that larger clusters are more reactive, but it explains this finding by multiple monomer-monomer contacts in the collision area.

## VI. CONCLUSIONS

Computer simulations corroborated that the Brownian kernel perfectly models pure diffusion-limited cluster aggregation. The significant deviations found between experimental data and the fitted Brownian kernel solution indicate that residual cluster-cluster interactions are not completely absent. This made it necessary to develop an alternative kernel that considers the monomer-monomer sticking probability explicitly and accounts for the possibility of multiple monomer-monomer contacts in the cluster collision area. The numerical solutions for the proposed kernel show an excellent agreement with the experimental data, obtaining a scaling exponent of $\lambda = 0.22$. The fact that a kernel that includes some concepts derived from reaction-limited cluster aggregation gives rise to solutions that agree excellently with the experimental data confirms that the system is almost but not purely diffusion-controlled. This implies that some residual interactions remain in the experimental system, although it was aggregated at an electrolyte concentration well above the critical coagulation concentration.

## ACKNOWLEDGMENTS

This work was supported by the Comisión Interministerial de Ciencia y Tecnología (CICYT, Project No. MAT97-1024). A.S. is grateful for financial support from the Gottlieb Daimler- and Karl Benz-Stiftung and G.O. for support from the European Union (Program: $\alpha$lpha, Proposal No. ALR/B7-3011/94.04-6.017.9).

[1] F. Family and D. P. Landau, in *Kinetics of Aggregation and Gelation*, edited by F. Family and D. P. Landau (North-Holland, Amsterdam, 1984).
[2] R. J. Hunter, *Foundations of Colloid Science* (Clarendon Press, Oxford, 1987).
[3] H. Sonntag and K. Strenge, *Coagulation Kinetics and Structure Formation* (Plenum Press, New York, 1987).
[4] M. von Smoluchowski, Phys. Z. **17**, 557 (1916).
[5] M. von Smoluchowski, Z. Phys. Chem. **92**, 129 (1917).
[6] P. G. J. van Dongen and M. H. Ernst, J. Stat. Phys. **50**, 295 (1988).
[7] A. A. Lushnikov, J. Colloid Interface Sci. **45**, 549 (1973).
[8] P. G. J. van Dongen and M. H. Ernst, Phys. Rev. A **32**, 670 (1985).
[9] M. L. Broide and R. J. Cohen, J. Colloid Interface Sci. **153**, 493 (1992).
[10] P. Meakin, Phys. Rev. Lett. **51**, 1119 (1983).
[11] P. Meakin, Phys. Rev. B **29**, 2930 (1984).
[12] M. Kolb, R. Botet, and R. Jullien, Phys. Rev. Lett. **51**, 1123 (1983).
[13] M. Kolb, Phys. Rev. Lett. **53**, 1653 (1984).
[14] D. A. Weitz and M. Oliveira, Phys. Rev. Lett. **52**, 1433 (1984).
[15] C. Aubert and D. S. Cannell, Phys. Rev. Lett. **56**, 738 (1986).
[16] M. L. Broide, Ph.D. thesis, Massachusetts Institute of Technology, 1988.
[17] J. K. G. Dhont, *An Introduction to Dynamics of Colloids* (Elsevier, Amsterdam, 1996).
[18] A. Fernández Barbero, A. Schmitt, M. A. Cabrerizo Vílchez, and R. Martínez García, Physica A **230**, 53 (1996).
[19] A. Fernández Barbero, M. A. Cabrerizo Vílchez, R. Martínez García, and R. Hidalgo Álvarez, Phys. Rev. E **53**, 4981 (1996).
[20] G. Odriozola, A. Schmitt, J. Callejas-Fernández, R. Martínez-García, and R. Hidalgo-Álvarez, J. Chem. Phys. **111**, 7657 (1999).
[21] P. Meakin, Z. Chen, and J. M. Deutch, J. Chem. Phys. **82**, 3786 (1985).
[22] P. N. Pusey and J. G. Rarity, Mol. Phys. **62**, 411 (1987).
[23] M. Y. Lin, R. Klein, H. M. Lindsay, D. A. Weitz, R. C. Ball, and P. Meakin, Phys. Rev. A **41**, 2005 (1990).
[24] M. Y. Lin, H. M. Lindsay, D. A. Weitz, R. Klein, R. C. Ball, and P. Meakin, J. Phys.: Condens. Matter **2**, 3093 (1990).
[25] T. Vicsek, *Fractal Growth Phenomena*, 2nd ed. (World Scientific, Singapore, 1992).
[26] M. Tirado-Miranda, A. Schmitt, J. Callejas-Fernández, and A. Fernández-Barbero, Langmuir **15**, 3437 (1999).
[27] M. Thorn and M. Seesselberg, Phys. Rev. Lett. **72**, 3622 (1994).
[28] L. A. Spielman, J. Colloid Interface Sci. **33**, 562 (1970).
[29] E. P. Honig, G. J. Roebersen, and P. H. Wiersema, J. Colloid Interface Sci. **36**, 97 (1971).
[30] A. Fernández Barbero, A. Martín Rodríguez, J. Callejas Fernández, and R. Hidalgo Álvarez, J. Colloid Interface Sci. **162**, 257 (1994).